Layered Nanostructures in Proton Conductive Polymers Obtained by Initiated Chemical Vapor Deposition

ARTICLE *in* MACROMOLECULES · AUGUST 2015

Impact Factor: 5.8 · DOI: 10.1021/acs.macromol.5b01145

6 AUTHORS, INCLUDING:

Roland Resel
Graz University of Technology
269 PUBLICATIONS **3,752** CITATIONS
SEE PROFILE

Bernd Cermenek
Graz University of Technology
5 PUBLICATIONS **1** CITATION
SEE PROFILE

Viktor Hacker
Graz University of Technology
115 PUBLICATIONS **935** CITATIONS
SEE PROFILE

Anna Maria Coclite
Graz University of Technology
23 PUBLICATIONS **259** CITATIONS
SEE PROFILE

Macromolecules

Article

pubs.acs.org/Macromolecules

Layered Nanostructures in Proton Conductive Polymers Obtained by Initiated Chemical Vapor Deposition

Christian Ranacher,[†] Roland Resel,[†] Priya Moni,[§] Bernd Cermenek,[‡] Viktor Hacker,[‡] and Anna Maria Coclite*[,†]

[†]Institute of Solid State Physics, NAWI Graz, and [‡]Institute of Chemical Engineering and Environmental Technology, Graz University of Technology, 8010 Graz, Austria

[§]Department of Materials Science and Engineering, Massachusetts Institute of Technology, Cambridge, Massachusetts 02139, United States

ABSTRACT: Proton conductive copolymers of 1*H*,1*H*,2*H*,2*H*-perfluorodecyl acrylate (PFDA) and methacrylic acid (MAA) have been synthesized by initiated chemical vapor deposition (iCVD). Detailed insights into the copolymers' molecular organization were gained through an X-ray-based investigation to serve as a starting point for systematic studies on the relation among proton conductivity and polymer structure. The method of copolymerization, iCVD, facilitated the tuning of the ratio between acidic −COOH groups, coming from MAA, and the hydrophobic matrix from the PFDA components. It was demonstrated that the copolymers crystallize into a bilayer structure, formed by the perfluorinated pendant chains of PFDA, perpendicular to the substrate surface. The MAA molecules form COOH-enriched regions among the bilayers—parallel to the substrate surface—which can act as ionic channels for proton conduction when the acid groups are deprotonated. The interplanar distance between the bilayer lamellar structures increases by the presence of MAA units from 3.19 to 3.56 nm for the MAA−PFDA copolymer with 41% MAA, therefore yielding to 0.4 nm wide channels. Proton conductivities as high as 55 mS/cm have been achieved for copolymers with 41% MAA fraction. Such ordered, layered nanostructures were never shown before for copolymers deposited from the vapor phase, and their anisotropy can be of inspiration for many applications beyond proton conduction. Moreover, the one-step copolymerization process has the potential to manufacture inexpensive, high quality membranes for proton exchange membrane fuel cells.

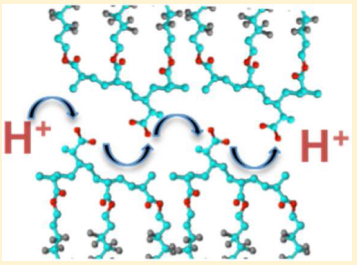

1. INTRODUCTION

The development of new and inexpensive electrolytes that can be successfully integrated in fuel cells as proton exchange membranes (PEM) is of high technological interest. A key feature required by such electrolytes is high proton conductivity, comparable to the actual benchmark, Nafion, low fuel crossover, and high stability. Cross-linked structures show high barrier properties against fuel crossover and improved stability.[1] The current paper aims to produce a membrane structure capable of driving high proton conductivity.

The fundamental processes of proton transport in proton conductive membranes have been largely investigated.[2,3] High proton conductivity is obtained when a large quantity of ionizable functional groups creates ionic channels for the proton or the hydrated proton, i.e. $H^+(H_2O)_n$, to migrate through the membrane.[4] During operation, the fuel cell is immersed in water, and thus the ionizable functional groups of the membrane should be located in a hydrophobic matrix to ensure mechanical integrity and limit the water uptake inside the PEM. Water and proton transport are linked and strongly dependent on the polymer chemical structure and/or morphology. Tuning the quantity and size of ionic channels in the hydrophobic matrix leads to optimum performance but requires a detailed knowledge of the chemical microstructure and nanoscale morphology of the membrane.

Nafion is known for its high proton conductivity and stability.[5] The molecule of Nafion is characterized by a hydrophobic polytetrafluoroethylene backbone chain and regularly spaced shorter perfluorovinyl ether side chains, each terminated by a strongly hydrophilic sulfonate ionic group. The peculiarity of Nafion is that when hydrated, it self-organizes into ionic and crystalline domains with a significant distribution in dimensions. Small-angle X-ray scattering (SAXS) studies on dry Nafion revealed only the presence of crystalline organization within the fluorocarbon matrix. However, when hydrated, a clear distinction between an ionic cluster peak and the semicrystalline PTFE-like matrix was observable.[2] The intensity of the ionic peak increases, and the position of the scattering maximum shifted to lower angles with increasing water content.

Initiated chemical vapor deposition (iCVD) has already proven to be a very promising technique to produce copolymers of methacrylic acid (MAA) and 1*H*,1*H*,2*H*,2*H*-perfluorodecyl acrylate (PFDA) (eq 1) with conductivities

Received: May 28, 2015
Revised: August 18, 2015

DOI: 10.1021/acs.macromol.5b01145
Macromolecules XXXX, XXX, XXX−XXX

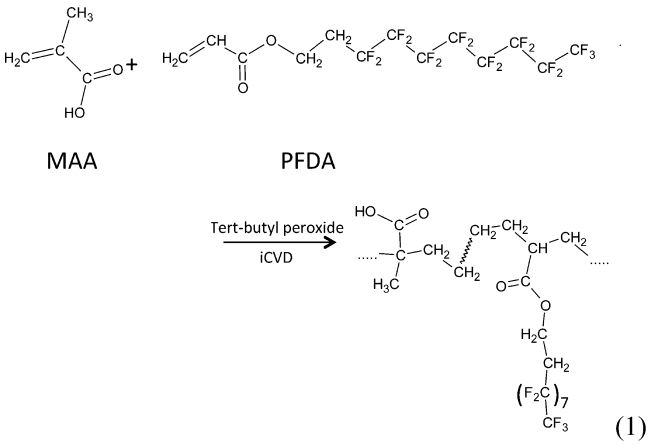

(1)

close to Nafion. MAA provides the ionizable carboxylic groups which are responsible for the proton conductivity, and PFDA provides the long and flexible hydrophobic chains.[6] Nevertheless, the internal morphology of the polymer chains was not investigated in detail.

Although carboxylic groups are less ionizable than sulfonic groups, they form short, strong hydrogen bonds with water, which has been demonstrated to be favorable for proton conductivity.[7] Using iCVD largely simplifies the copolymerization of monomers with different solubilities, like MAA and PFDA. The iCVD polymerization occurs in a completely dry vacuum chamber fed with a thermally labile initiator and the monomer(s). The initiator is thermally decomposed into free radicals by a filament heated to temperatures in the range of 200−300 °C. Temperatures in this range are high enough to decompose only the labile peroxide O−O bond of the initiator, while the monomer(s) can travel intact in the reactor and adsorb on the substrate surface, which is cooled to a temperature in the range of 25−60 °C. Because of the low vapor pressure of the monomers used in the iCVD processes, the probability of initiator radicals and monomer reacting in the gas phase is very low. Kinetic models instead show that a heterogeneous reaction takes place between the initiator radicals and the monomer adsorbed at the substrate temperature.[8−10] Arrhenius plots of the polymer deposition rate as a function of substrate temperature result in activation energies highly comparable to the activation energies calculated by adsorption experiments, implying that iCVD is a surface-driven and more specifically adsorption-limited process. The rest of the polymerization steps, chain growth and thin film formation, take place on the surface as well. The high volatility of the initiator and of its fragments ensures only limited degree of inclusion of the initiator fragments in the growing polymer chain, except for the initiation and termination phase.[10] Further details on the polymerization mechanism of iCVD are given in many reviews recently published.[11,12]

Some PTFE-like lamellar structures were observed both for the PFDA homopolymer, deposited by iCVD, as well as in the perfluorinated backbone of Nafion.[2,13] In the Nafion copolymer, the lamellar structure is retained with a lower crystallinity ratio and a lower bilayer interplanar distance. The objective and novelty of this study are to understand how the structural aggregation of the MAA−PFDA copolymers changes from the PFDA homopolymer. Therefore, a detailed structural investigation of these proton conductive copolymers was performed by various X-ray scattering techniques including X-ray reflectivity (XRR), specular and off-specular X-ray diffraction (XRD), and grazing incidence X-ray diffraction (GIXD).

To the authors' knowledge, this is the first time that such detailed structural investigation is made on iCVD copolymers. Therefore, it is expected that the outcome of this study can also be used for other comparative studies on iCVD copolymers, not necessarily in the field of proton conductivity.

2. EXPERIMENTAL SECTION

MAA−PFDA copolymers were deposited by initiated chemical vapor deposition (iCVD) on silicon substrates (Siegert Wafer) up to thicknesses of 130 ± 15 nm.

The depositions were performed in a custom-built cylindrical vacuum reactor with a diameter of 36 cm and a height of 5.5 cm. Schematics of a typical iCVD reactor are present in the literature.[11,12] The reactor had a removable 2.5 cm thick quartz lid, which allowed laser interferometry (He−Ne Laser, Thorlabs, λ = 633 nm) for *in situ* thickness control. To evacuate the chamber, a rotary pump (Pfeifer Duo 5M) was used, and the pressure was monitored with a MicroPirani gauge (Balzers). The pressure during the depositions was kept at 800 mTorr.

The hydrophilic monomer (methacrylic adic, MAA, 99%, Aldrich), the hydrophobic comonomer (1*H*,1*H*,2*H*,2*H*-perfluorodecyl acrylate, PFDA, 97%, Aldrich), and the initiator (*tert*-butyl peroxide, TBPO, 98% Aldrich) were used without any further purification and flowed into the reactor chamber without prior mixing. While the initiator vaporizes at room temperature, the MAA and PFDA were heated to 70 and 80 °C, respectively. Swagelok needle valves were used to control the flow rates. The nitrogen flow rate was controlled with a mass flow controller (MKS).

To create the initiator radicals, the labile peroxide bond of the initiator was thermally broken by a filament array, which consisted of 12 parallel nickel chromium wires (Goodfellow), placed 2.5 cm above the substrate. The filaments were heated up to 284 ± 3 °C with a dc power supply (Heinzinger PTN 350-5). The substrate temperature was controlled with a chiller/heater (Thermo Scientific Accel 500 LC) to 50 ± 5 °C. All temperatures were monitored by type K thermocouples (Omega Engineering).

The experiments were carried out with a constant initiator flow rate of 1.00 ± 0.05 sccm and a constant PFDA flow rate of 0.30 ± 0.03 sccm while the MAA and nitrogen flow rates were adjusted to keep the total flow rate at 5.7 sccm. The flow rates are summarized in Table 1.

Table 1. Flow Rates Used for the Growth of MAA−PFDA Polymers by iCVD and the Ratios of Monomer Partial Pressure (P_M) and Saturation Pressure (P_{sat}) for the Two Monomers at the Substrate Temperature

sample	MAA flow rate [sccm]	PFDA flow rate [sccm]	TBPO flow rate [sccm]	N_2 flow rate [sccm]	P_M/P_{SAT} MAA	P_M/P_{SAT} PFDA
A	0.0	0.3	1.0	4.4		0.126
B	0.3	0.3	1.0	4.1	0.006	0.126
C	0.6	0.3	1.0	3.8	0.013	0.126
D	1.0	0.3	1.0	3.4	0.021	0.126
E	1.4	0.3	1.0	3.0	0.030	0.126
F	3.0	0.0	1.0	1.7	0.064	

The thicknesses of the films were measured *ex situ* by variable angle spectroscopic ellipsometry (VASE, M-2000S, J.A. Woolam). The measurements were collected at three different angles (65°, 70°, and 75°) in the wavelength range of 200−1000 nm. A three-layer optical model was applied, consisting of the silicon substrate, the native SiO_2 layer (1.7 nm), and the film bulk layer. The film bulk layers were modeled by the Cauchy function with Urbach tail.

The chemical composition and structure of the films were investigated by Fourier transform infrared (FT-IR) spectroscopy (Bruker IFS 66v/S). The measurements were carried out in

DOI: 10.1021/acs.macromol.5b01145
Macromolecules XXXX, XXX, XXX−XXX

transmission mode. For this purpose silicon wafers transparent under IR light were used as substrates. The spectra were recorded from 4000 to 400 cm^{-1} with a resolution of 4 cm^{-1}. A nonlinear least-squares regression was performed on the absorption peak at 1690−1760 cm^{-1} using two Gaussian components with the "Multiple Gauss Peaks" procedure of the qti-Plot software. The area under each Gauss component was used to determine the percentage of MAA and PFDA in the film (referred to as F_{MAA} and F_{PFDA}, respectively).

To investigate the structure of the films, various X-ray scattering techniques were used. To observe Bragg peaks, the films were investigated by specular (ψ = 0°) and off-specular (ψ > 0°) X-ray diffraction (XRD) using a goniometer with Eulerian geometry (Philips PW1830-ATC3, λ = 0.228 975 nm). Grazing incidence X-ray diffraction (GIXD) measurements were carried out at the Helmholtz Zentrum Berlin, using beamline KMC-2, with an incident angle of 0.13°, wavelength of 0.100 nm, and a Bruker 2D cross-wire detector.

Bragg peaks and Laue oscillations at small scattering angles were investigated in the X-ray reflectivity (XRR) regime (PANalytical, Empyrean, λ = 0.154 178 nm). The exact peak position and the full width at half-maximum intensity (fwhm) were calculated by fitting the Bragg peaks with a Gaussian curve. Kiessig fringes were observed at low roughness as a result of the interference from the X-ray beam scattered from the air−polymer and the polymer−silicon interface. The latter features can be used to determine the film thickness. Since each of the mentioned methods (XRD, XRR, GIXD) uses X-ray sources with different wavelengths, we report the diffraction patterns in terms of the scattering vector q instead of the scattering angle 2θ. The advantage of using the scattering vector is that the position does not depend on the wavelength of the X-ray source, and therefore it is easier to compare the plots derived from different techniques. The scattering vector, $\vec{q}$, is defined as the difference between the incoming wavevector and the outgoing wavevector $\vec{q} = \vec{k} - \vec{k'}$, and the magnitude is calculated as $q = (4\pi/\lambda) \sin\theta$. The magnitude of $\vec{q}$ is correlated with the interplanar distance d via $q = 2\pi/d$. In specular conditions, the scattering vector is perpendicular to the film surface, and therefore we indicate it with q_z. In GIXD measurements, the scattering vector $\vec{q}$ has not only a contribution in the z-direction, q_z, but also in the in-plane directions (x and y) which is summarized as q_p.[14]

Advancing and receding water contact angles (WCA) were measured using a Ramé-Hart 200 goniometer with the sessile drop method. The contact angles were measured by depositing a 2 μL droplet on the surface, then increasing it in steps of 0.25−4 μL, and then decreasing it in steps of 0.25 μL until the droplet's retreat was observed. Advancing angles were considered as the maximum observed angle just before the droplet advanced. Receding contact angles were measured in correspondence of the drop profile just before the contact surface reduction. Each WCA value was averaged from measurements of eight drops with an estimated maximum error of 6%.

The film morphology and the surface roughness were investigated by atomic force microscopy (Veeco Dimension 3100) in tapping mode, using antimony (n) doped Si tips (Bruker).

The in-plane proton conductivity was measured by electrochemical impedance spectroscopy (Gamry Instruments, Reference 600) with a four-point probe. An alternating voltage signal of RMS 50 mV was applied in the frequency range from 0.1 to 10 000 Hz, and 5 points per decade were recorded. The open circuit voltage was measured for 50 s before the measurements to adjust the working point. The samples were cut into strips with widths between 1.1 and 1.4 cm and were mounted in a BT-110 conductivity clamp (Scribner Associates). Five measurements for each sample were carried out at room temperature. The measurements were performed in approximately 400 mL of ultrapure water (17.4 MΩ cm). The conductivity was calculated using eq 2.

$$\sigma = \frac{1}{R_{mem}} \frac{L}{WT} \tag{2}$$

where L is the distance between the inner voltage-sensing electrodes (0.425 cm), W is the membrane width, and T is the membrane thickness. The values for the membrane resistance (R_{mem}) were taken from the real component of the impedance, where the measured resistance equals the resistance of the parallel circuit of the membrane and the solution. The measured water resistance was approximately 270 kΩ. Since the film thickness was only 1 μm, the measured resistance of the membranes was rather high, ranging between 48 and 138 kΩ. Therefore, the water resistance was measured additionally after every measurement and used to correct the value of the measured membrane resistance as reported in eq 3.

$$R_{mem} = \left(\frac{1}{R_{tot}} - \frac{1}{R_{water}} \right)^{-1} \tag{3}$$

Measurements of proton conductivity on thicker membranes would have resulted in a smaller error bar due to a bigger difference between water and membrane resistance.[15] On the other hand, membranes thicker than 1 μm were difficult to achieve due to the low deposition rate obtained with the chosen conditions. For proton conductivity measurements, the MAA−PFDA copolymers were deposited on a porous PTFE carrier film (Goodfellow), with a thickness of 63 μm, a porosity of 84%, and a pore size of 0.45 μm. The PTFE substrate was used for its flexibility to facilitate the handling of the membranes in the conductivity clamps. The total resistivity PTFE plus water matched the resistance of the pure water; therefore, the resistivity of the PTFE carrier was neglected.

3. RESULTS AND DISCUSSION

Copolymers of PFDA−MAA with different ratios of fluorinated over carboxylic groups were obtained by changing the monomer flow rates. Generally, it is reported in the literature that the copolymerization kinetics are strongly dependent on the fraction f of each monomer that is adsorbed on the surface.[16] The amount of each monomer adsorbed on the surface can be related to the ratio between the monomer partial pressure (P_M) and the saturated vapor pressure (P_{sat}) at the substrate temperature.[8,9] Therefore, the fraction of MAA adsorbed on the surface was estimated from eq 4.

$$f_{MAA} = \frac{\left(\frac{P_M}{P_{sat}}\right)_{MAA}}{\left(\frac{P_M}{P_{sat}}\right)_{MAA} + \left(\frac{P_M}{P_{sat}}\right)_{PFDA}} \times 100 \tag{4}$$

Table 1 summarizes the flow rates used and the corresponding P_M/P_{sat} values. The corresponding fraction of MAA adsorbed on the surface f_{MAA} is reported in Table 2.

The deposition rates (Table 2) were ranging from 2.3 to 6.5 nm/min, which are similar to the deposition rates previously obtained for PFDA crystalline polymers.[13] The deposition rates increased linearly with f_{MAA} between 5 and 19%.

Table 2. Depositions Rates, MAA Fraction on the Surface (f_{MAA}) as Calculated from the P_M/P_{sat} Ratio, and MAA Fraction in the Copolymer (F_{MAA}), Determined by Calculating the Fraction of the Area of the COOH FTIR Peak

sample	deposition rate [nm/min]	f_{MAA} [%]	F_{MAA} [%]
A	2.3	0	0
B	3.1	5	12 ± 7
C	4.6	9	27 ± 3
D	5.7	15	41 ± 1
E	6.5	19	45 ± 1
F	3.7	100	100

DOI: 10.1021/acs.macromol.5b01145
Macromolecules XXXX, XXX, XXX−XXX

Figure 1a shows the FTIR spectra of the deposited films at different MAA fractions. In the spectrum of the MAA

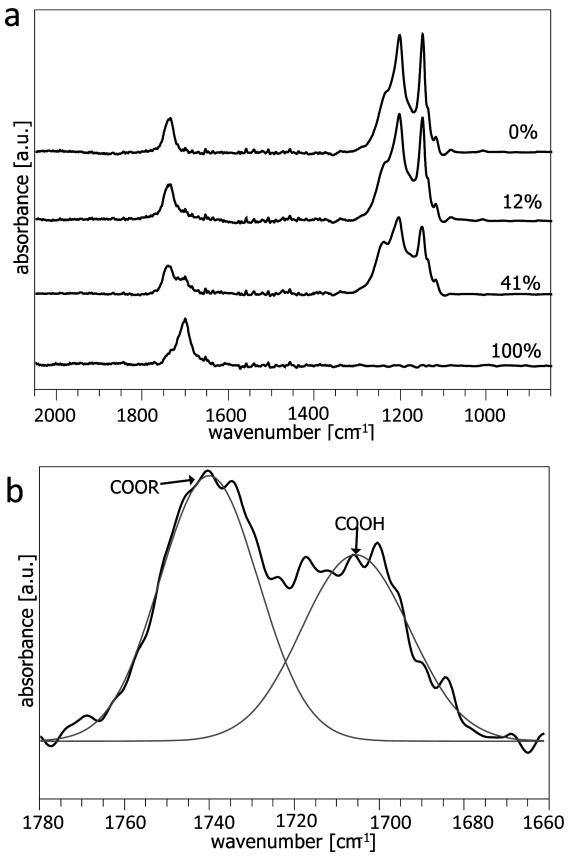

Figure 1. (a) FTIR spectroscopy of different copolymers in the range from 2050 to 850 cm^{-1}. The labels give the actual fraction F_{MAA} in the polymer. A shift in the carbonyl peak can be observed from 1706 cm^{-1} (MAA−COOH group) to 1740 cm^{-1} (PFDA−COOR group), where with R we indicate the esteric pendant chain of PFDA. The areas of the individual contributions to the peak depend on the fraction of each monomer in the copolymer. (b) Nonlinear least-squares regression of the carbonyl peak in the copolymer with F_{MAA} = 41%. The actual fraction of MAA and PFDA in the copolymer was determined by calculating the ratio of the area of the individual Gauss component (COOH or COOR) to the total area.

homopolymer (F_{MAA} = 100%), the absence of the C−O absorptions (1050−1150 cm^{-1}) suggests that the free radical polymerization resulted in ≈1% or less incorporation of the initiating *tert*-butoxy fragments in the deposited film. This is consistent with the initiator fragments being the end groups for polymer chains of reasonable length. As the MAA fraction in the copolymer increases, the absorptions of the fluorinated pendant chains (symmetric and asymmetric CF_2 stretching at 1205 and 1233 cm^{-1}, respectively, and CF_2−CF_3 stretching at 1150 cm^{-1}) and of the functional group COOR (R indicates the esteric pendant chain of PFDA) at 1741 cm^{-1} decrease in intensity. The opposite occurs for the absorption of the COOH group at 1706 cm^{-1}. Figure 1b shows a fit of the carbonyl peak using two Gaussian components for the COOH and COOR groups. Since the COOH groups come only from MAA and the ester groups COOR only from PFDA, the area under each Gauss component was used to determine the percentage of MAA and PFDA in the film (referred to as F_{MAA} and F_{PFDA}, respectively). The last column of Table 2 shows the values of F_{MAA} calculated from the FTIR COOH contribution. Depending on the reactivity of the monomer, the actual percentage of monomer units in the copolymer is usually different from the one calculated with the P_M/P_{sat} (f_{MAA}).[6] It is noteworthy noticing that F_{MAA} increases with f_{MAA} with a slope of 2.5. Generally, the copolymer composition (in terms of F_{MAA} and F_{PFDA}) is similar to the fraction of each monomer adsorbed on the surface (f_{MAA} and f_{PFDA}).[6,16] In this case, instead, F_{MAA} grows much faster than f_{MAA}, meaning that the percentage of MAA incorporated in the copolymer is much higher than the one of PFDA. This could be ascribed to the slow kinetics of polymerization of PFDA in regime of crystallinity.[13] Indeed, PFDA has been shown to polymerize in two different regimes, resulting in crystalline or amorphous films. The two regimes are characterized by very different kinetics. While amorphous films can be deposited at rates >100 nm/min, crystalline films have never been observed at deposition rate >20 nm/min.

Figure 2 shows the XRR patterns of the films deposited with different MAA content (F_{MAA}). PFDA homopolymers showed

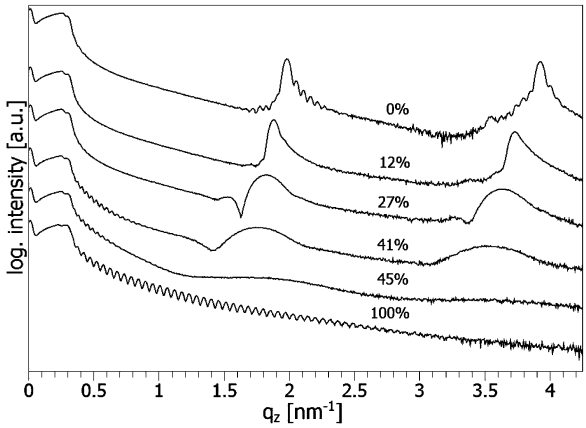

Figure 2. XRR measurements of the polymers. The labels give the percentage of MAA in the polymer (F_{MAA}). The PFDA homopolymer and the MAA−PFDA copolymers showed first- and second-order Bragg peaks from the (001) plane which shifted to a lower scattering vector q_z and thus to higher plane distances with increasing MAA fraction. The Bragg peaks decrease in intensity with increasing MAA fraction due to the loss of crystallinity. The intensity is plotted on a logarithmic scale, and the curves are shifted for clarity.

strong first- and second-order Bragg peaks of the (001) plane, at q_z = 1.98 nm^{-1} and q_z = 3.92 nm^{-1}, respectively. These peaks correspond to an interplanar distance of 3.19 ± 0.02 nm. The peaks occur due to the organization of the fluorinated chains into a bilayer structure (Scheme 1).

It was shown before that PFDA crystallizes into an ordered lamellar structure, specifically a smectic B phase.[13,17,18] The interplanar distance of 3.19 nm corresponds to the length of a double layer of fluorinated chains. On the left- and right-hand side of the Bragg peaks, in Figure 2, Laue oscillations were observed. These oscillations occur due to the finite size of the crystals and can be used to estimate the crystal size. The intensity of the Bragg peaks decreases with increasing MAA fraction in the copolymer, which indicates some loss of crystallinity. Other authors have also shown that copolymers of PFDA do not retain the crystallinity degree of the PFDA homopolymers when a comonomer is added.[19] The Bragg peaks are also broadened which indicates that the crystallite size decreases. The MAA homopolymers showed no Bragg peaks, as

DOI: 10.1021/acs.macromol.5b01145
Macromolecules XXXX, XXX, XXX−XXX

Scheme 1. (a) Bilayer Lamellar Structure of the PFDA Homopolymer; (b) Hypothetical Model for the MAA–PFDA Lamellar Structure;[a] (c) Schematics of the Distribution of the Crystalline Lamellar Domains in the Entangled Coils of the Polymer Chains

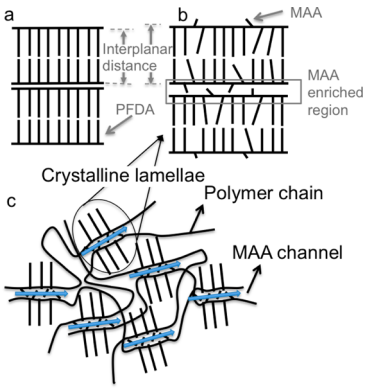

[a]The MAA orientation toward the outside is hypothesized to explain the increase of the length of the repeat unit and thus the interplanar distance. The bending of the PFDA chains in the empty space where the MAA has turned on the outside would explain why we observe lower crystallinity and smaller crystallite sizes.

expected. The observed fringes in the XRR profile of the MAA polymer are Kiessig fringes.[20] The period of these fringes can be used to determine the film thickness. These fringes disappear for films with a MAA fraction ≤27% most likely due to roughening of the surface, as confirmed later by AFM investigations.

It can be observed in Figure 2 that the Bragg peaks shift to lower angles with increasing MAA fraction, which demonstrates an increase of the interplanar distance. The interplanar distance, d, calculated from the first-order Bragg peak is plotted in Figure 3 as a function of F_{MAA} (%).

Since the peak of the film with 45% MAA was very weak and broad, it was not possible to obtain a proper fit. The fwhm was used to estimate the crystal size (t) using the Scherrer equation

$$t = \frac{2\pi}{\Delta q} \tag{5}$$

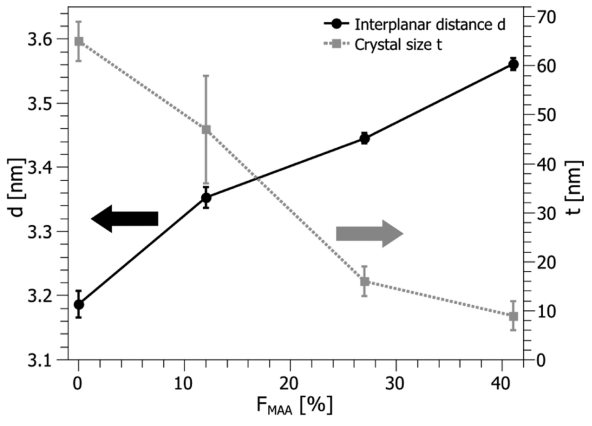

Figure 3. Plane distance and crystal size as a function of the MAA percentage in the copolymer (F_{MAA}). The plane distance increased with the MAA fraction, while the crystal size is decreasing due to the more disordered copolymer structural aggregation and the resulting loss of the crystallinity.

with Δq as the width of the Bragg peak. The estimated crystal size is plotted in Figure 3 as a function of F_{MAA}. The interplanar distance significantly increased from 3.19 to 3.56 nm, while the estimated crystal size decreased from 65 to 9 nm. The fact that the interplanar distance increases with the MAA fraction proves that there is no phase separation between MAA and PFDA domains in the copolymer. In the case of a phase separation between the crystalline PFDA and the amorphous MAA domains, the peak would decrease in intensity with increasing MAA fraction but would always be observed at the same q_z. Kinetic studies have proven that MAA–PFDA copolymers have a moderate alternate composition in terms of MAA units linked to PFDA units.[5] The propensity of a growing polymeric chain, terminating with a monomer unit A, to add a monomer A over the other monomer B is defined as reactivity ratio of the monomer A, r_A.[21] Similarly, a reactivity ratio for the monomer B (r_B) can be defined. If the product $r_A r_B$ is lower than 1, the copolymer composition is estimated to be close to alternating. The kinetic investigations on the reactivity ratio for the present set of conditions resulted in r_{MAA} higher than r_{PFDA}, while the product $r_{MAA}r_{PFDA}$ is still below 1. In detail, applying the Fineman–Ross method,[22] we obtained r_{MAA} = 2.1 and r_{PFDA} = 0.22, with $r_{MAA}r_{PFDA}$ = 0.42. The high MAA reactivity ratio is in accordance with the high inclusion of MAA versus PFDA in regime of crystallinity, as discussed previously. It is worthy mentioning that copolymers of PFDA were not deposited before in conditions that drive crystallinity;[6,19,23] therefore, a comparison with previously obtained reactivity ratios is difficult. An alternate polymer composition, without phase separation between MAA and PFDA domains, is difficult to achieve with other techniques due to the large difference in solubilities of the comonomers. This problem is circumvented with the iCVD method, as evidenced by obtaining $r_{MAA}r_{PFDA} < 1$.

In Scheme 1b, a model is proposed for the MAA–PFDA copolymer structure. We hypothesize that the MAA molecule turns on the outside of the bilayer structure, increasing the length of the repeat unit and thus the interplanar distance of the copolymer. The fluorinated chain bends over to fill the empty space, which leads to a more disordered state. The cluster-network model that was proposed for hydrated Nafion describes the formation of ionic clusters that are interconnected by ionic channels.[2] The X-ray investigation of the MAA–PFDA polymer structure was not carried out in water, and therefore it was not possible to observe the peaks relative to the ionic clusters. Ionic channels are instead already evident in the dry state in the hypothesized model of Scheme 1b. When the MAA molecules are oriented outside the bilayers, only MAA is present among the repeating units. The measured increase of the interplanar distance for the copolymer with 41% MAA is 0.37 nm, which is approximately the length of the MAA molecule. This means that in the copolymer with 41% MAA fraction the MAA molecules stand upright, leading to a wider hydrophilic interlayer. The water molecule has a diameter of 0.27 nm; therefore, a hydrophilic interlayer as large as 0.37 nm would facilitate the passage of water through the membrane and act as an ionic channel to improve the proton conductivity.

To investigate if there is a preferred orientation of the crystals or if they are oriented randomly, off-specular XRD measurements were carried out at different tilt angles (Figure 4). Only crystals with net planes perpendicular to the scattering vector contribute to the Bragg peak signal, whereby peaks at ψ = 0° occur only from interplanar distances, which are oriented perpendicular to the surface. At ψ = 0° the observed peaks

DOI: 10.1021/acs.macromol.5b01145
Macromolecules XXXX, XXX, XXX–XXX

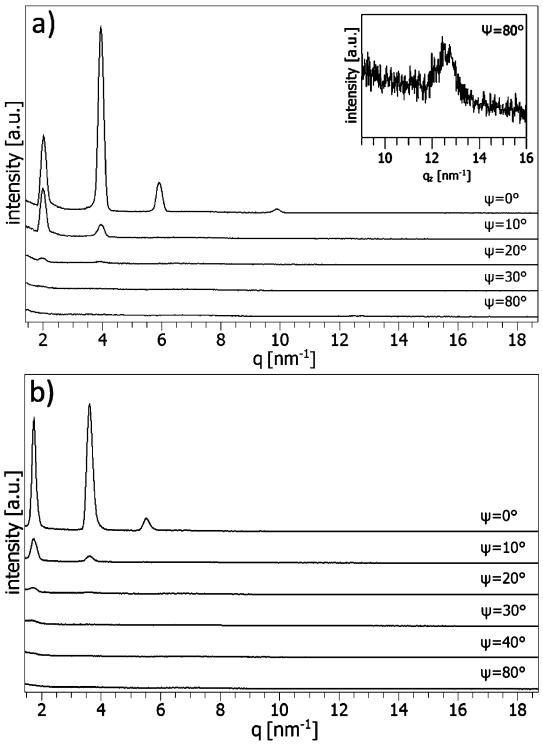

Figure 4. $\theta-2\theta$ scans at different tilt angles of the PFDA homopolymer (a) and a MAA−PFDA copolymer with 12% MAA fraction (b). The Bragg peaks disappear at a tilt angle of 30° and 40°, respectively, which demonstrates the preferred orientation of the polymer crystals. The inset in (a) shows the 9−16 nm^{-1} range of the $\theta-2\theta$ scans at a tilt angle of 80°. The small in-plane peak at q_z = 12.5 nm^{-1} (d = 0.50 nm) indicates an in-plane organization of the polymers. This in-plane peak was not observed for the copolymer films.

occur due to the orientation of the layered structure (Scheme 1a).[13] The peaks observed for the PFDA homopolymer (Figure 4a) at 1.98 and 3.92 nm^{-1} are the same first- and second-order Bragg peaks visible also in Figure 2. The third order is and fifth orders are also visible in Figure 4a at 5.92 and 9.88 nm^{-1}. For the copolymer with 12% MAA fraction, first- and second-order peaks were observed at 1.88 and 3.73 nm^{-1} analogous to the XRR measurements as well as a third-order peak at 5.60 nm^{-1}. The intensity of the Bragg peaks of the bilayer structure quickly decreases with an increase in the tilt angle, and the peaks are no longer visible at ψ = 30° and ψ = 40°, respectively, or higher. It is evident that there is indeed a preferred orientation of the layers at ψ = 0° with orientation distributed in the range of 0−40°, as illustrated in Scheme 1c. The inset of Figure 4a shows a zoom of the diffractogram measured at ψ = 80°. A small peak is visible at q_z = 12.5 nm^{-1}, which indicates an in-plane order. According to the literature, the in-plane structure of PFDA is hexagonal.[13,24] The measured peak at q_z = 12.5 nm^{-1} corresponds to an interplanar distance of 0.50 nm. This in-plane distance leads to a lattice constant of 0.58 nm (Scheme 2).

In Figure 4b we report the measurement done on the copolymer with F_{MAA} = 12%. The preferential orientation of the crystal perpendicular to the substrate surface implies that the ionic channels are oriented parallel to the substrate surface. The preferred orientation of the layers was observed for the copolymers with $F_{MAA} \leq 41\%$.

Scheme 2. Hexagonal In-Plane Structure of PFDA Homopolymers[a]

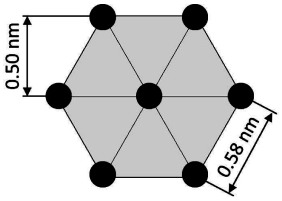

[a]The measured interplanar distance of 0.50 nm corresponds to a lattice constant of 0.58 nm.

To gain more information about the crystal structure, GIXD measurements were performed, and the results are shown in Figure 5. The strong Bragg peak for the pure PFDA polymer at

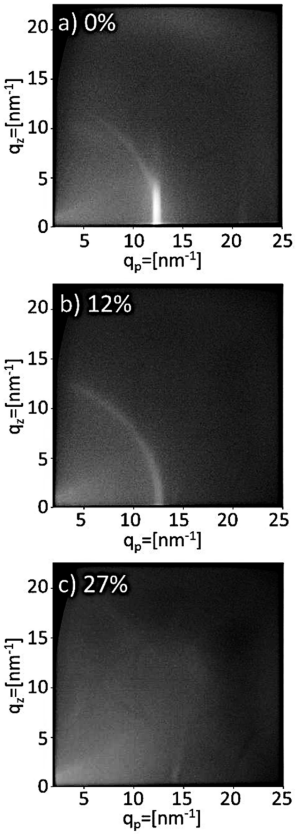

Figure 5. Grazing incidence X-ray diffraction (GIXD) measurements. The labels correspond to the actual fraction F_{MAA} in the polymer. The PFDA homopolymer (a) showed a Bragg rod at q_p = 12.5 nm^{-1}, which indicates a 2D crystal without correlation between the crystal planes. The logarithmic scale allows to detect a Debye−Scherrer ring, barely visible at 0% MAA but clearly visible for the 12% MAA. It results from randomly oriented crystals. (c) At higher MAA fraction also the Debye−Scherrer ring disappears, and the films show only amorphous scattering, which means that there is no order.

q_p = 12.5 nm^{-1} matches with the observed XRD peak at ψ = 80° and confirms that there is an in-plane order with a plane distance of 0.50 nm. The fact that the GIXD measurement for the PFDA homopolymer has shown a Bragg rod rather than a Bragg peak means that PFDA crystallizes in a 2D crystal where the planes are not correlated. All these data confirm that PFDA crystallizes in a smectic B phase (Scheme 3b).

DOI: 10.1021/acs.macromol.5b01145
Macromolecules XXXX, XXX, XXX−XXX

Scheme 3. (a) PFDA−MAA Copolymers Crystallize in a Smectic a Phase with a Layered Structure and a Preferred Orientation of the Polymer Chains; (b) Pure PFDA Polymers Crystallize in a Smectic B Phase Which Has Besides a Layered Structure and a Preferred Orientation of the Crystals Also an In-Plane Structure

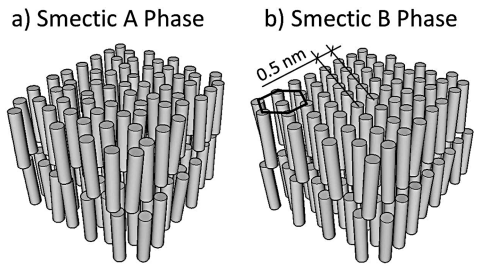

The Bragg rod is no longer observable for the 12% MAA film, meaning that there is no in-plane order for the MAA−PFDA copolymers. At higher MAA fraction no Bragg peaks were observed. The absence of in-plane order but the evidence of lamellar organization with preferential orientation (Bragg peaks) in the copolymers are characteristics of a smectic A phase (Scheme 3a). Weak Debye−Scherrer rings are visible for the samples with F_{MAA}= 0% and 12%, which demonstrates that there are small randomly orientated crystals in the films.

The surface morphology of the films was investigated with AFM in tapping mode. Figure 6 shows the AFM topographical

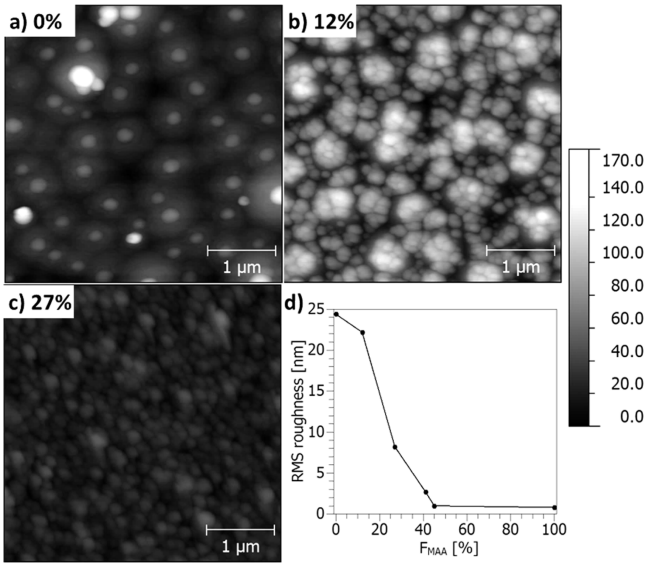

Figure 6. Topographical AFM investigation of the films (a−c). The label corresponds to the MAA fraction in the polymer (F_{MAA}). The height scale was kept constant. The PFDA homopolymer showed sharp high features but had a lower density of features compared to the copolymer. The observed size of the features as well as the RMS roughness (d) of the films decreased with increasing MAA fraction in the polymer.

images of the PFDA homopolymer and the copolymer with 12% and 27% MAA fraction. In contrast to the homopolymer, which showed the presence of islands at defined sites, the copolymer showed a more molehill-like morphology. Large island shape aggregations are characteristics of crystalline domains, also observed in other studies on PFDA homopolymers.[13] The observed size of the features as well as the RMS roughness of the film decreased with increasing MAA fraction in the polymer. The RMS roughness of the PFDA homopolymer was 24.4 nm and decreased for the copolymers with the MAA fraction. Such morphology evolution was observed also for other crystalline copolymers of PFDA.[19] Similarly to this case, the surface features decreased in size but increased in density, resulting in an overall smoothening of the film. The reason for the higher density of island was ascribed to the higher number of nucleation sites obtained when the total gas pressures stay constant but the comonomer flow rate increases. The copolymers with high MAA fraction, e.g. with 45% MAA, were smooth and had a roughness of 1 nm. This confirmed the XRR observation, where Kiessig fringes were only visible for films with 41% MAA or higher. The loss of island aggregation at fraction of MAA higher than 41% can be related with the transition from the crystalline to the amorphous state.

Since water and proton conductivity are strongly connected, an ideal polymer structure would give chain reorientation in water to allow the transport. An indirect observation of chain reorientation in our copolymers was derived from dynamic water contact angle measurements. Advancing (WCA_{adv}) and receding (WCA_{rec}) contact angles on the copolymer films and on the PFDA homopolymer are shown in Figure 7. The contact

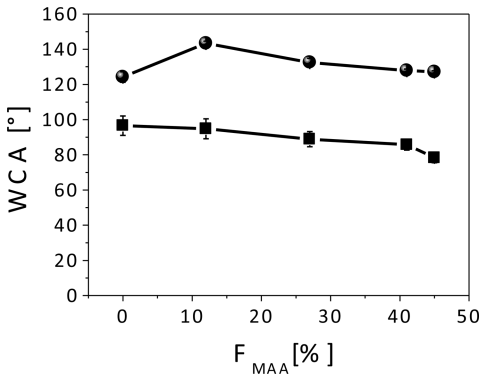

Figure 7. Advancing (●) and receding (■) water contact angles measured for the MAA−PFDA copolymers, varying the MAA fraction. The advancing WCA increases from the PFDA homopolymer to the 12% MAA copolymer, probably due to the relative loss of crystallinity, which results in a more disordered surface with higher fraction of CF_3 groups on the surface. By further increasing the hydrophilic MAA, the WCA decreases. The receding WCA showed a steady decrease.

angle on the MAA homopolymer decreased rapidly with time, and the film was almost instantly diluted by the water. Therefore, there are no measurements available for the MAA homopolymer. The advancing contact angle for the PFDA homopolymer was 124° and increased for the copolymer with 12% MAA to 143°. This increase could be caused by the change in the smectic phase. Since the 12% MAA is less crystalline, the chains are more randomly oriented, and the more hydrophobic CF_3 groups can move toward the surface, increasing the WCA. In the PFDA homopolymer, the CF_3 groups are hidden in the bilayer structure; therefore, even if the hydrophobic monomer component is higher, this leads to a lower WCA. Similar behavior was observed for other MAA−PFDA copolymers.[6] By further increasing the hydrophilic MAA components, the advancing WCA slightly decreased to 127°. The receding WCA for the PFDA homopolymer was 97° and steady decreased with the MAA fraction, leading to an increase in

DOI: 10.1021/acs.macromol.5b01145
Macromolecules XXXX, XXX, XXX−XXX

hysteresis from 27° to 49°. The increase in hysteresis can be due to several factors. (i) The copolymers are less crystalline than the PFDA homopolymer. This means they can reorient more easily to expose hydrophilic groups inside the drop of water. (ii) The copolymers are very likely to have surface chemical heterogeneities due to the presence of the MAA units in addition to PFDA. (iii) The surface roughness can also affect this behavior,[25−27] especially if the spacing among the surface features is high relative to their depth, so water can fill the gaps and stick on the surface. The latter effect should be more visible at low density of island features on the surface, i.e., at low MAA fraction, considering Figure 6. At high MAA fractions, therefore the effects of crystallinity loss and chemical heterogeneities prevail.

We measured the in-plane proton conductivity with electrochemical impedance spectroscopy. Preliminary results are shown in Figure 8. As a reference, also the conductivity of

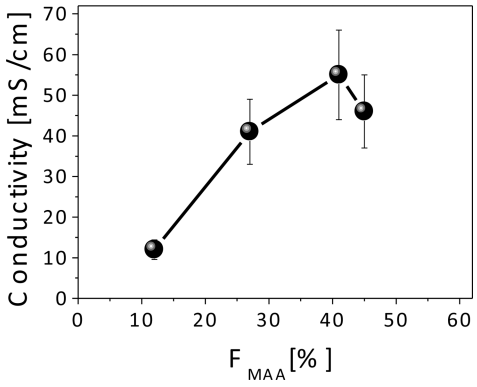

Figure 8. Proton conductivity (σ) of MAA−PFDA copolymers, measured at room temperature in ultrapure water, including standard deviation based on five measurements for every sample. The error was estimated at 40% for all the values due to the low thickness of our membranes.

Nafion115 was measured in the same conditions as for the copolymers, and it resulted in 126 mS/cm, which is in agreement with literature values.[5] The amount of ionizable groups in the copolymer with 12% MAA fraction is low, and therefore the conductivity was only 12 mS/cm for this copolymer. However, the conductivity was significantly higher for films with a higher MAA fraction and reached a maximum of 55 mS/cm for the copolymer with 41% MAA fraction. In addition to the higher fraction of ionizable groups, the larger width of the ionic channels, which was discussed previously, could have led to this high proton conductivity. Further studies are under investigation to corroborate this hypothesis and clarify the proton transport mechanism in the MAA−PFDA copolymers, e.g., to confirm that the bilayer-ionic channel structure is retained also in water and when the copolymers are deposited on PTFE instead of Si wafers. Since the proton conductivity was measured at room temperature, it can be expected that it would be even better at higher temperatures.

It is worth noticing that even if the channels are parallel to the surface, they may still be distributed in the polymer coils in a way that leads to through-plane interconnections and conductivity, as illustrated in Scheme 1c. It was shown in the literature that the orientation of the bilayers can be tuned with the depositions conditions[13] (i.e., filament temperature), and therefore it should be possible to orient the ionic channels in through-plane directions.

4. CONCLUSIONS

Proton conductive polymers, which can be used as proton exchange membranes in fuel cells, were synthesized out of hydrophilic (MAA) and hydrophobic (PFDA) monomers. These monomers have very different solubilities; therefore, the use of a solventless technique, initiated chemical vapor deposition (iCVD), highly simplified the copolymerization. The polymers were investigated with various X-ray-based methods in order to gain insights into the microscopic structure. Proton conduction is strictly related to the polymer chain organization. For this reason, a detailed structural characterization of the MAA−PFDA copolymers can be extremely beneficial as starting point for systematic studies and advances on proton conductive membranes.

The MAA−PFDA copolymers crystallize in a bilayer lamellar structure, where the perfluorinated chains of the PFDA monomer unit orient toward themselves and the bulk of the polymer chains plus the MAA units are exposed outward. The interplanar distance between the bilayer lamellar structures increases by the presence of MAA units from 3.19 nm for the PFDA homopolymer to 3.56 nm for the MAA−PFDA copolymer with 41% MAA. The increase in the interplanar distance proved that there is indeed a crystalline copolymer structure and not a phase separation between the crystalline PFDA and the amorphous MAA domains. From these results, a hypothetical model for the MAA−PFDA bilayer structure was proposed, which also describes the formation of MAA-enriched regions between the bilayers. These regions can act as ionic channels, when the COOH groups of the MAA units are depronated. X-ray diffraction measurements at different tilt angles demonstrated that the chains of the homopolymer and the copolymer have a preferred orientation perpendicular to the surface, which implies that the channels are oriented in-plane.

Dynamic water contact angle measurements showed that the polymer chains have a high mobility, which can be beneficial for the proton conductivity. Electrochemical impedance spectroscopy proved that the MAA−PFDA copolymers are capable of transporting protons and have shown very promising conductivities for the copolymers with high MAA fraction up to a maximum of 55 mS/cm for the copolymer with 41% MAA. Different acid monomers may be used to create bigger channels as well as more ionizable acid groups (e.g., $-SO_3H$) may be beneficial to improve the proton conductivity. Further tests will be done also to assess the stability and the fuel crossover in these membranes.

AUTHOR INFORMATION

Corresponding Author

*E-mail: anna.coclite@tugraz.at (A.M.C.).

Notes

The authors declare no competing financial interest.

ACKNOWLEDGMENTS

The authors thank the Helmholtz-Zentrum Berlin for the allocation of synchrotron radiation beamtime. We are grateful to Daniel Többens for providing assistance in using beamline KMC-2 and Christian Röthel, Paul Christian, and Ingo Salzmann for supporting the experiments. Stephan Weinberger is kindly acknowledged for his help with the proton conductivity measurements. The financial support of the FWF-ProCVD project (P 26993-N19) is gratefully acknowl-

DOI: 10.1021/acs.macromol.5b01145
Macromolecules XXXX, XXX, XXX−XXX

edged. Prof. Karen K. Gleason is kindly acknowledged for the interesting scientific discussions.

REFERENCES

(1) Guo, Q.; Pintauro, P. N.; Tang, H.; O'Connor, S. *J. Membr. Sci.* **1999**, *154*, 175−181.
(2) Mauritz, K. A.; Moore, R. B. *Chem. Rev.* **2004**, *104*, 4535−4585.
(3) Hsu, W. Y.; Gierke, T. D. *J. Membr. Sci.* **1983**, *13*, 307−326.
(4) Arimura, T.; Ostrovskii, D.; Okada, T.; Xie, G. *Solid State Ionics* **1999**, *118*, 1−10.
(5) Neburchilov, V.; Martin, J.; Wang, H.; Zhang, J. *J. Power Sources* **2007**, *169*, 221−238.
(6) Coclite, A. M.; Lund, P.; Di Mundo, R.; Palumbo, F. *Polymer* **2013**, *54*, 24−30.
(7) Hensley, J. E.; Way, D. J. *J. Power Sources* **2007**, *172*, 57−66.
(8) Lau, K. K. S.; Gleason, K. K. *Macromolecules* **2006**, *39*, 3695−3703.
(9) Lau, K. K. S.; Gleason, K. K. *Macromolecules* **2006**, *39*, 3688−3694.
(10) Baxamusa, S. H.; Gleason, K. K. *Chem. Vap. Deposition* **2008**, *14*, 313−318.
(11) Coclite, A. M.; Howden, R. M.; Borrelli, D. C.; Petruczok, C. D.; Yang, R.; Yagüe, J. L.; Ugur, A.; Chen, N.; Lee, S.; Jo, W. J.; Liu, A.; Wang, X.; Gleason, K. K. *Adv. Mater.* **2013**, *25*, 5392−5423.
(12) Reeja-Jayan, B.; Kovacik, P.; Yang, R.; Sojoudi, H.; Ugur, A.; Kim, D. H.; Petruczok, C. D.; Wang, X.; Liu, A.; Gleason, K. K. *Adv. Mater. Interfaces* **2014**, *1*, 1400117.
(13) Coclite, A. M.; Shi, Y.; Gleason, K. K. *Adv. Funct. Mater.* **2012**, *22*, 2167−2176.
(14) Birkholz, M. *Thin Film Analysis by X-Ray Scattering*; Wiley: New York, 2006.
(15) Dedmond, E.; Cooper, K. Application Note − Effect of Solution Conductivity on In-Plane Membrane Conductivity Measurement; http://www.scribner.com/files/knowledgebase.
(16) Lau, K. K. S.; Gleason, K. K. *Macromol. Biosci.* **2007**, *7*, 429−434.
(17) Honda, K.; Morita, M.; Otsuka, H.; Takahara, A. *Macromolecules* **2005**, *38*, 5699.
(18) Volkov, V. V. *Polymer* **1992**, *33*, 1316.
(19) Yague, J. L.; Gleason, K. K. *Macromolecules* **2013**, *46*, 6548−6554.
(20) Kiessig, H. *Ann. Phys.* **1931**, *402*, 769.
(21) Odian, G. G., Ed.; *Principles of Polymerization*, 4th ed.; Wiley-Interscience: Hoboken, NJ, 2004.
(22) Fineman, M.; Ross, S. D. *J. Polym. Sci.* **1950**, *5* (2), 259−62.
(23) Perrier, S.; Jackson, S. G.; Haddleton, D. M.; Ameduri, B.; Boutevin, B. *Macromolecules* **2003**, *36* (24), 9042−9.
(24) Amadei, C. A.; Yang, R.; Chiesa, M.; Gleason, K. K.; Santos, S. *ACS Appl. Mater. Interfaces* **2014**, *6*, 4705−4712.
(25) Cassie, A.; Baxter, S. *Trans. Faraday Soc.* **1944**, *40*, 546.
(26) Welzel, P. B.; Weis, I.; Scharz, G. *Colloids Surf., A* **1998**, *144*, 229.
(27) Murakami, D.; Jinnai, H.; Takahara, A. *Langmuir* **2014**, *30* (8), 2061−2067.

DOI: 10.1021/acs.macromol.5b01145
Macromolecules XXXX, XXX, XXX−XXX